Received: 25 January 2018 | Revised: 4 August 2018 | Accepted: 8 August 2018

DOI: 10.1002/joc.5841

International Journal of Climatology RMetS

RESEARCH ARTICLE

Spatial and temporal changes in the frequency and magnitude of intense precipitation events in the southeastern United States

Walker J. Skeeter | Jason C. Senkbeil | David J. Keellings

Department of Geography, University of Alabama, Tuscaloosa, AL

Correspondence
Walker J. Skeeter, Department of Geography, University of Alabama, Farrah Hall Room 200, 513 University Blvd, Tuscaloosa, AL 35487.
Email: wjskeeter@crimson.ua.edu

Intense precipitation events (IPE; 99th percentile) in the southeastern United States from 1950 to 2016 were analysed temporally, spatially, and synoptically. The study area was partitioned into latitudinal and physiographic regions to identify subregions that experienced significant changes in IPE frequency or intensity. Furthermore, the spatial synoptic classification (SSC) was used to ascertain what surface weather types are associated with IPEs. Additionally, in conjunction with the SSC, surface forcing mechanisms for the 30 most extreme subregional IPEs were studied to uncover the surface synoptic conditions responsible for IPEs. Results revealed that IPEs increased in frequency and intensity on an annual basis for the southeastern United States. Seasonal results indicated that IPE frequency only increased in the fall. Subregional results reveal that latitudinally, IPEs became more common in the northern latitudes of the study area, while physiographically, significant increases in IPE frequency were most pronounced in areas inland from the Atlantic Coastal Plain. An increase in the annual number of IPEs associated with moist tropical (MT) days was identified across the study area, but was more prevalent in the central and north central latitudinal regions, and areas inland from the Atlantic Coastal Plain outside of the Appalachian Mountains. This MT increase was possibly caused by more common northwards and inland intrusion of these types of IPEs. While moist moderate (MM) and transitional (TR) days were most commonly associated with IPEs, these weather types did not have significant trends. The surface forcing mechanisms most commonly associated with the strongest IPEs were tropical events, followed by stationary fronts and concentric low-pressure systems.

KEYWORDS

climate, intense precipitation, southeastern United States, spatial, surface-based observations, synoptic, temporal

1 | INTRODUCTION

While considerable uncertainty still exists regarding whether precipitation amounts will increase globally, regionally, annually, and seasonally in the future (IPCC, 2013), it is often anticipated that as the climate warms, intense precipitation events (IPEs) will become more common as well as more extreme (Trenberth *et al*., 2003; Emori and Brown, 2005; Janssen *et al*., 2014; Prein *et al*., 2016). In the United States, heavy precipitation events have shown evidence of increasing trends in both recurrence and intensity, particularly in the northeast United States (Collow *et al*., 2016), and also with mesoscale convective systems (Prein *et al*., 2017). The frequency and magnitude of the most extreme floods has increased dramatically in Europe and the United States for the period from 1980 to 2009 (Berghuijs *et al*., 2017). Furthermore, Mallakpour and Villarini (2017) found evidence of increasing frequency of heavy precipitation events for most regions of the United States. IPEs and flooding can be detrimental to both natural landscapes and human populations. Increases in the occurrence of IPEs are likely to lead to greater flooding and landslide events, which have the potential to adversely impact society and infrastructure (McGuire, 2010). In the United States, heavy precipitation events and flooding have caused considerable property damage despite federal and local policy initiatives to mitigate impacts over time (Brody *et al*., 2011).

There is a large volume of literature surrounding observed and expected trends in IPEs. IPEs are expected to become more common over time, due principally to changes in atmospheric circulation and increasing atmospheric moisture that are expected to accompany a warming climate (Emori and Brown, 2005; Chou *et al*., 2012; Fischer and Knutti, 2016). It is predicted that overall precipitation intensity will increase by approximately 7% worldwide (Trenberth *et al*., 2003) with a marked increase in heavy precipitation events, although this change is expected to be characterized by regional variability (IPCC, 2013). Hourly precipitation extremes in the contiguous United States will increase significantly in areas that have access to abundant moisture, but will decrease abruptly in moisture-limited regions (Prein *et al*., 2016). IPEs and more episodic precipitation regimes also have the potential to increase the chance for drought and consecutive dry day periods (Anderegg *et al*., 2013), although Trepanier *et al*. (2015) found that many stations in the south central United States have experienced shorter periods of consecutive dry days.

Modelling studies of precipitation intensity are not particularly skilled at replicating inherent differences in precipitation at different latitudes (O'Gorman and Schneider, 2009), or areas with varied topography and elevations (Jones *et al*., 2015). Models may be overestimating future changes in intensity by exceeding the amount of atmospheric moisture that is available (Sugiyama *et al*., 2010). A lack of temporal homogeneity in experienced changes is also apparent, with Nickl *et al*. (2010) finding that across global land surfaces the first half of the 20th century (1902–1949) saw an increase in annual precipitation while the period from 1949 to 1993 saw an overall decrease in annual precipitation. That trend again reversed itself, with the period of 1992–2002 showing an increase of approximately 0.75–2.1 mm/year. Despite issues in model skill extreme precipitation indices, and subsequently the frequency of intense events, are expected to continue increasing throughout the next century (Janssen *et al*., 2014).

Due to these findings and uncertainties, an implicit understanding of past surface synoptic mechanisms and upper atmospheric synoptic patterns associated with IPEs is essential for accurate modelling and prediction (O'Gorman and Schneider, 2009; Nickl *et al*., 2010; Sugiyama *et al*., 2010; Pathirana *et al*., 2014). This is especially true for the southeastern United States (SeUS), which is subjected to many different synoptic and mesoscale influences on IPEs throughout the year. Schumacher and Johnson (2006) explored the seasonality of IPEs in the SeUS, finding that while the northern United States experiences IPEs almost exclusively during the warm season, the SeUS experiences IPEs throughout the entire year due to relatively warm winter temperatures and access to warm water. Furthermore, the SeUS is a region that has been characterized by a muted or absent warming signal in temperature during 1951–1975 (Pan *et al*., 2013; Rogers, 2013; Meehl *et al*., 2015), but a warming signal is thought to have returned in more recent decades (Grose *et al*., 2017). Although this region has generally lagged behind model projections of temperature increase, relatively fewer studies have examined changes in precipitation events over time in the region. Thus, the importance of understanding the ingredients necessary for IPEs, and historical precipitation and IPE trends is of great concern in the context of future model projections and climate change verification.

Previous climatological IPE research in the SeUS has used synoptic approaches both seasonally and annually. Keim (1996) classified IPEs (defined as any 2-day period of three or more inches of liquid equivalent precipitation) for eight weather stations across the SeUS as either frontal, tropical, or air mass events, and found that frontal events were the dominant forcing mechanism in the SeUS. Keim (1997) used similar methodology, with 27 observation stations and 92 years of data, and found that in the SeUS, the Gulf Coast received the largest number of intense events, while the Appalachians and Texas received the fewest. The study also found that the Southeast Coast, particularly South Carolina, exhibited a small decline in the total number of intense events per year. This Southeast Coast decline was confirmed by Frich *et al*. (2002), and again by Powell and Keim (2015), who additionally found that across the SeUS IPEs have become more common, while higher extreme minimum and lower extreme maximum temperatures have occurred, narrowing diurnal temperature ranges across much of the region. The eastern portion of their study area, particularly South Carolina, was again found to defy the increasing IPE trend that the rest of the region is experiencing. Kunkel *et al*. (2012) examined all 5-year return events across the United States, and determined that for the Southeast, tropical systems comprised 51% of these anomalous events, while frontal systems were responsible for 34% of such events. Outside of the Southeast, the study showed that for the entire contiguous United States, frontal events accounted for the majority of intense events, at 54%, emphasizing a notable difference between the Southeast's synoptic mechanisms when compared to the rest of the country. Furthermore, Moore *et al*. (2015) conducted a synoptic radar-based study, which utilized 24-hr multi-sensor precipitation analyses as a means of avoiding the spatial variability that is introduced by using point-based observation stations. IPEs were defined as 99th and 99.9th percentile events in the SeUS. It was found that non-tropical IPEs form in both strongly synoptically forced scenarios, and weakly synoptically forced scenarios. The precipitation totals of IPEs that form under a weak synoptic regime are more difficult to forecast.

In this research, IPE trends were evaluated for 56 surface observation stations across a 10-state region of the SeUS. The specific objectives were (a) to examine annual, seasonal, and physiographic/latitudinal subregional trends in IPEs for changes in both frequency and intensity and (b) to understand the surface weather types, conditions, and forcing mechanisms responsible for IPEs both spatially and temporally by utilizing the spatial synoptic classification (SSC) scheme, which has not been used in previous IPE research. The emphasis on regional and subregional areal trends via latitude and physiography in combination with SSC weather types helps to distinguish this research on IPEs from previous studies within the SeUS. Furthermore, the definition of an IPE in this research accounts for both precipitation duration and intensity marking another unique attribute. It is hoped that results from this research can help meteorologists, climatologists, and hydrologists identify the common conditions associated with forecasting IPEs in the context of understanding long-term IPE trends in an evolving state of climatic change and variability.

2 | METHODS

2.1 | Defining IPE and IPE trends

Daily precipitation totals from 1950 to 2016 were collected from the National Climate Data Center (NCDC) for 56 surface stations across the SeUS. The definition of SeUS that is used in this research is all states south of 39°43′N latitude (the northern border of the state of Maryland), and east of the Mississippi River (Figure 1), excluding the Florida Peninsula south of 30°N latitude. The Florida Peninsula was omitted due to its unique precipitation regime owing to different forcing mechanisms than the SeUS for much of the year. Each station had at least 95% data coverage, and 41 were first-order (National Weather Service [NWS] staffed) stations. The remaining stations were second-order (not NWS staffed) located at regional airports (4), research

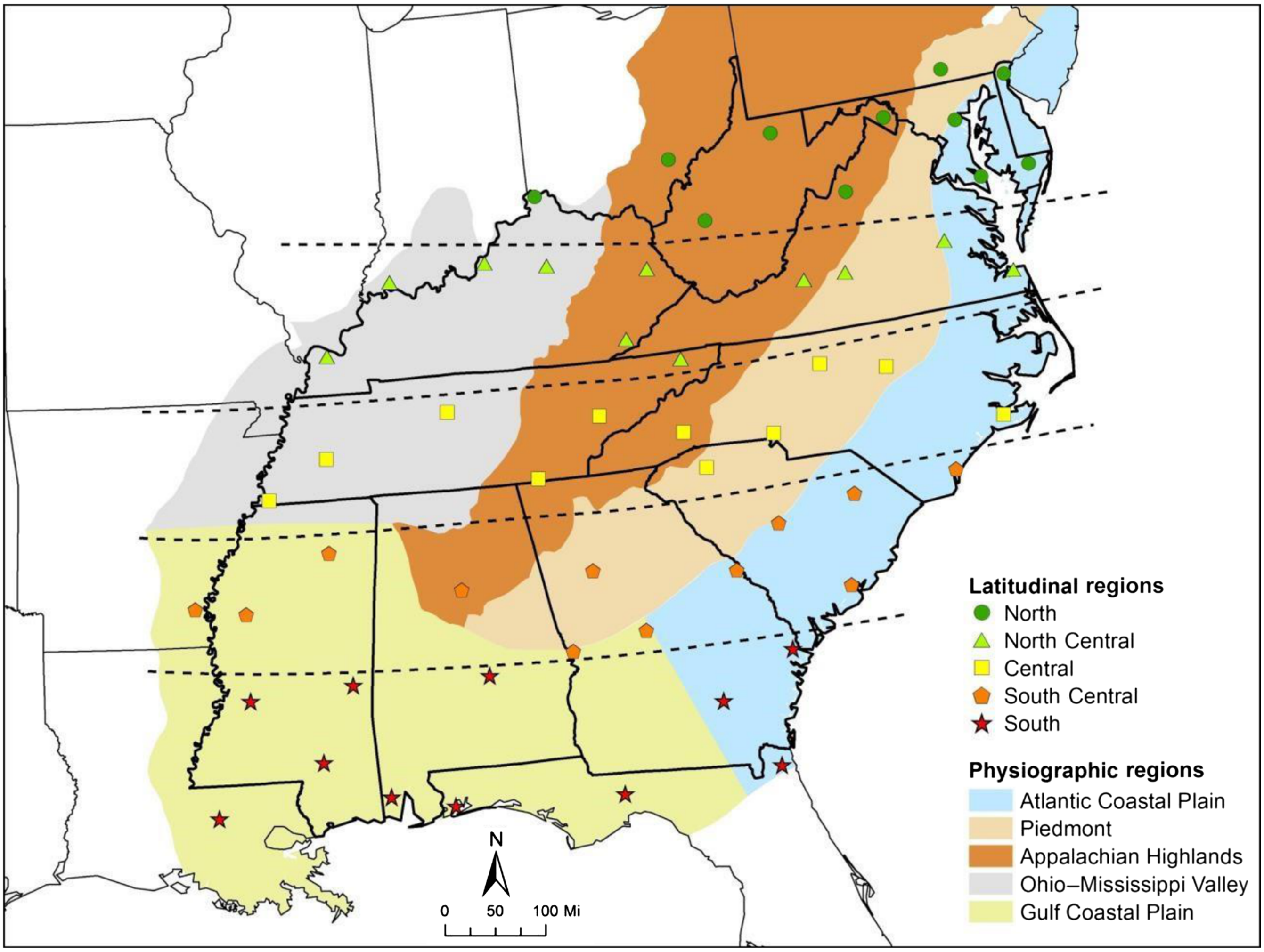

FIGURE 1 Study area showing all stations grouped according to latitude and physiographic subregion [Colour figure can be viewed at wileyonlinelibrary.com]

centres/universities (2), or independently operated locations (9). Four stations were included outside but adjacent to the aforementioned boundaries to assist in the creation of interpolated maps.

A script was written in R to identify all distinct precipitation events. A precipitation event was defined as any set of consecutive days with measurable precipitation, in order to capture both the intensity, and hydrological significance of events, similar to Agel *et al*. (2015). One limitation to delineating events this way is the timing of precipitation from different events not aligning with the 24 hr/day (e.g., multi-day events with continuous or near continuous periods of precipitation). It is possible to have a prolonged period of precipitation lasting several days, and it is also possible to have a short but IPE contained within 1 day or covering 2 days. An objective of this research was to analyse IPEs both spatially and temporally by frequency and intensity. Therefore, steps were taken to avoid over-representing longer duration, but not otherwise intense events, while ensuring equal representation of shorter duration but otherwise intense events. The amounts from both events could possibly be the same, but the shorter, more intense event produces more runoff and has greater flood potential. A simple adjustment equation was created to partition fair representation of both short- and long-term events,

$$\left(\frac{\text{Event total}}{\text{Event length}}\right) + \text{most intense daily total} = \text{adjusted strength}.$$

Taking the average of the total precipitation produced by a given event reduces the total associated with exceedingly long-term events, while adding the highest daily total to the average allows any long-term events that were associated with an embedded intense single day total to be represented.

Once each distinct event was identified and adjusted, precipitation events were assigned a z-score, based on the adjusted event strength. Typical of research using extremes, the overwhelming majority of precipitation events were low in adjusted strength resulting in a gamma distribution. After z-scores were assigned, each location's 99th percentile events were identified and extracted. These 99th percentile events were defined as IPEs, and were used as the basis for statistical analysis. The lower bound adjusted IPE strength for each station was mapped using a kriging interpolation in GIS for the entire study area (Figure 2). This represents the spatial variability in the minimum adjusted strength for events to be considered an IPE. As previously described, the objective was to fairly represent duration and intensity for IPEs. For this reason the 99th percentile z scores at each station were designated as IPEs instead of the 99th percentile event totals which could be biased towards duration. Trend analysis using the 99th percentile totals across the entire region showed almost identical statistical significance; therefore, the 99th percentile z scores were retained. This method was deemed most appropriate because using 99th percentile strength events relative to each location creates a similar sample size of IPEs at each location. A static absolute threshold method similar to that utilized by Keim (1996) was considered, but preliminary research showed this methodology leads to skewed sample sizes between coastal and inland areas with coastal areas having significantly more events above the threshold.

For trend identification and significance, ordinary least squares (OLS) regression was used to test for annual and seasonal linear trend significance in both IPE frequency and intensity across the entire region and subregions. Due to the nature of extremes, some years at individual stations were characterized by anomalous occurrences of IPEs, while other years had no IPEs. Inherently this caused the data at individual stations to be non-normally distributed. When combining the individual stations into subregions for analysis, very few aggregate distributions became non-normally distributed. Furthermore, plots of the studentized residuals against the unstandardized predicted values revealed that all subregion results displayed linear relationships, and plots of residuals against predicted values showed constant variance for all subregions. Additionally, Durbin–Watson values ranged from 1.6 to 2 for all subregions. Nonparametric Mann–Kendall slope tests were used in conjunction with OLS regression for subregions with non-normally distributed data, and no juxtapositions between OLS regression and Mann–Kendall significance results (i.e., significant OLS trend, but non-significant Mann–Kendall trend, vice versa) were identified.

2.2 | Defining IPE subregions within the SeUS

The study area spans almost 10° of latitude comprised of several distinct physiographic regions with varying topography. Land areas within each state are organized into state climatic divisions by the National Climatic Data Center (NCDC) based on similar physiography and climatic characteristics to facilitate analysis (U.S. Climate Divisions). Similarly here, latitude subregions of similar annual precipitation totals and physiographic subregions of similar topography were used to gain a better understanding of what areas have shown the strongest contributions within the larger SeUS study area. Latitude and physiographic provinces have been utilized in previous climate or hydroclimate research. Senkbeil *et al*. (2017) utilized latitude regions to examine weather type change over time in the eastern United States, while Barros *et al*. (2017) studied decadal-scale influences on hydrologic drought within physiographic provinces of the SeUS.

For the latitudinal subregions, five north–south regions were identified with sample sizes of 11 or 12 stations (see Figure 1). For the physiographic subregions, a USGS physiography map with both major and minor physiographic provinces within the study area was downloaded via ArcGIS

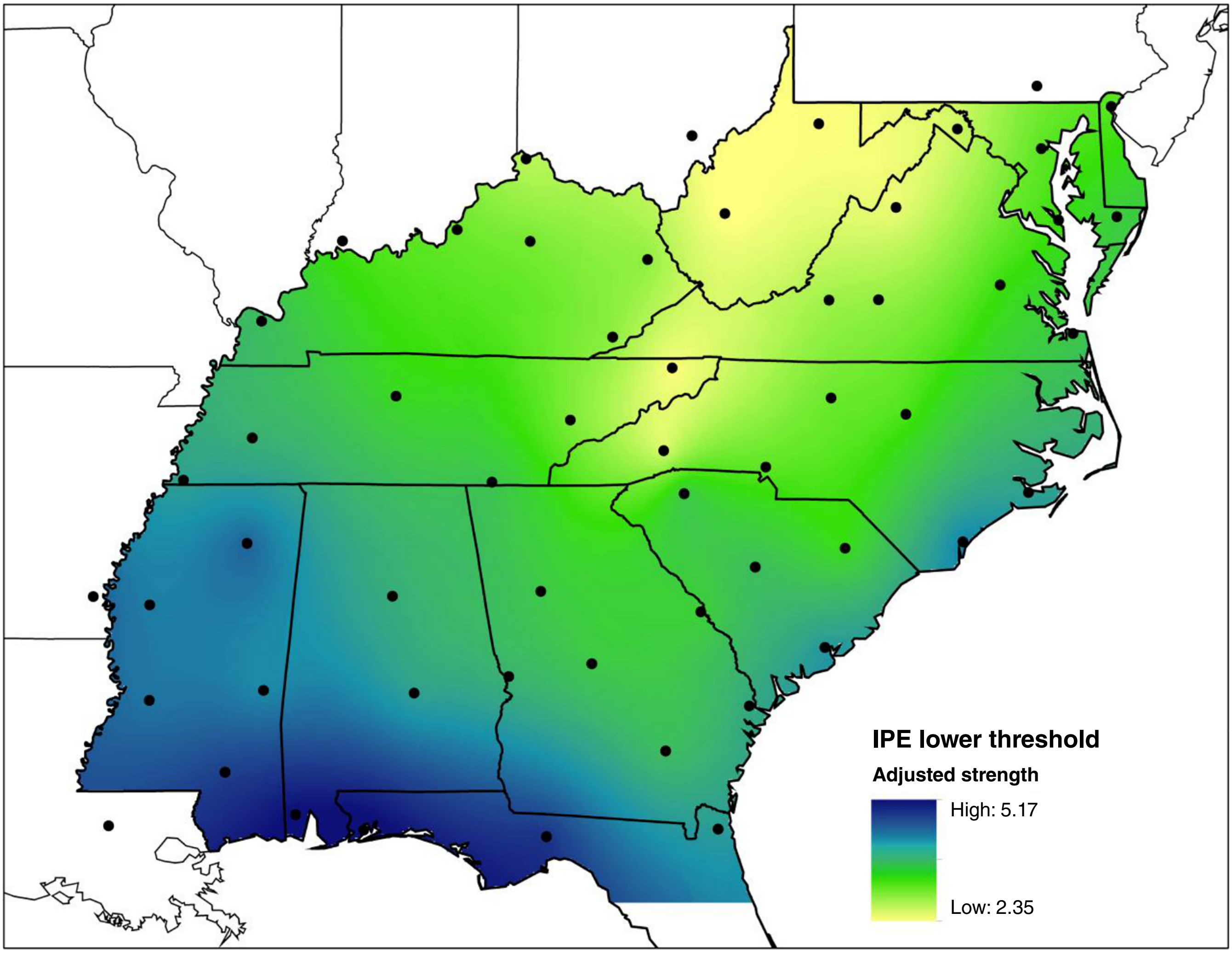

FIGURE 2 Kriging interpolated surface showing the lower bound adjusted strength for an event to be considered an IPE across the study area [Colour figure can be viewed at wileyonlinelibrary.com]

online (Fenneman and Johnson, 1946). In order to allow a meaningful sample size within each region, only the major physiographic regions were used with a small modification to create five physiographic provinces. These provinces (as well as the total number of stations within them) are the Atlantic Coastal Plain (15), Gulf Coastal Plain (13), Piedmont (7), Appalachian Highlands (13), and Ohio–Mississippi Valley (8). In order to create equal sample sizes, the Ohio–Mississippi Valley subregion was constructed by combining five stations of the Interior Low Plateau region with three stations on the northern reaches of the Gulf Coastal Plain (see Figure 1). The three northern Gulf Coastal Plain stations that were added to the Ohio–Mississippi Valley subregion had more in common climatologically with the five Interior Low Plateau region's stations due to their inland location away from mesoscale convective warm season processes, such as the sea breeze. Methods for regional trend identification and significance were identical to those for the entire study area.

2.3 | The SSC and surface forcing mechanisms

This research utilizes the SSC (Sheridan, 2002) as a means of documenting the type of surface weather associated with IPEs. The SSC is a daily surface weather type classification scheme that has been used in over 90 published climate articles to date. Although primarily used in heat and human health research and recently with extreme temperature events (Allen and Sheridan, 2016), the SSC has been used previously in studies of urban precipitation enhancement (Dixon and Mote, 2003; Ashley *et al*., 2012; Bentley *et al*., 2012). It has not been used with precipitation extremes on the synoptic scale but could be particularly useful as a way of discovering conditions and analogues associated with IPEs that could be used in future forecasts.

The SSC has seven weather type classes with descriptions found on the SSC homepage (http://sheridan.geog.kent.edu/ssc.html). The descriptions in this research are modified for the SeUS and only include weather types that produce precipitation:

- Moist moderate (MM): cloudy, mild, and humid, MM is commonly a modified moist polar or moist tropical (MT) weather type that has strayed from its source regions. It is common along stationary frontal boundaries or with mid-latitude cyclones.
- Moist polar (MP): cool or cold, cloudy, and humid, often with light stratiform precipitation associated with mid-latitude cyclones or other frontal systems.
- MT: warm or hot and humid, with common origins from the Gulf of Mexico, Caribbean, or tropical Atlantic. It also has additional extreme categories of MT+ and MT++ representing oppressive hot and humid days. These were all combined into one MT category for this research.
- Transition (TR): one weather type yields to another, common along frontal boundaries or other processes where there are considerable changes between the 6 hr observations used for daily classification.

Each IPE was assigned a daily SSC classification. If a station among the 56 used was not an SSC station (Figure 3), the closest SSC station was used to assign the weather type manually. When assigning SSC classifications to individual IPEs that span multiple days, the day within the IPE that experienced the most precipitation was used to assign the SSC weather type. This technique was used because the day within an event with the most precipitation is inherently the best representative of an IPE. This had the potential to introduce bias in IPEs that experienced a relatively uniform distribution of precipitation per day, but that is an uncommon occurrence. Based on a sample of six randomly selected stations from different regions used in this research, only 6.6% of IPEs experienced precipitation totals in which the two most intense days of the event were within 2.54 cm (1 in.) of each other. That percentage dropped to 2.7% when the threshold was lowered to 1.25 cm (0.5 in.). Generally, IPEs have a clearly defined most intense day.

In addition to the SSC classification, surface forcing mechanisms for the 30 most intense IPEs in each physiographic region (150 total) were manually classified utilizing archived surface maps based on the most intense daily total of the events using methods similar to Keim (1996). Each event was assigned to one of the following classifications, based on what was determined to be the primary cause of the IPE: air mass, frontal (warm, cold, or stationary), low pressure (concentric, or with frontal influence), tropical

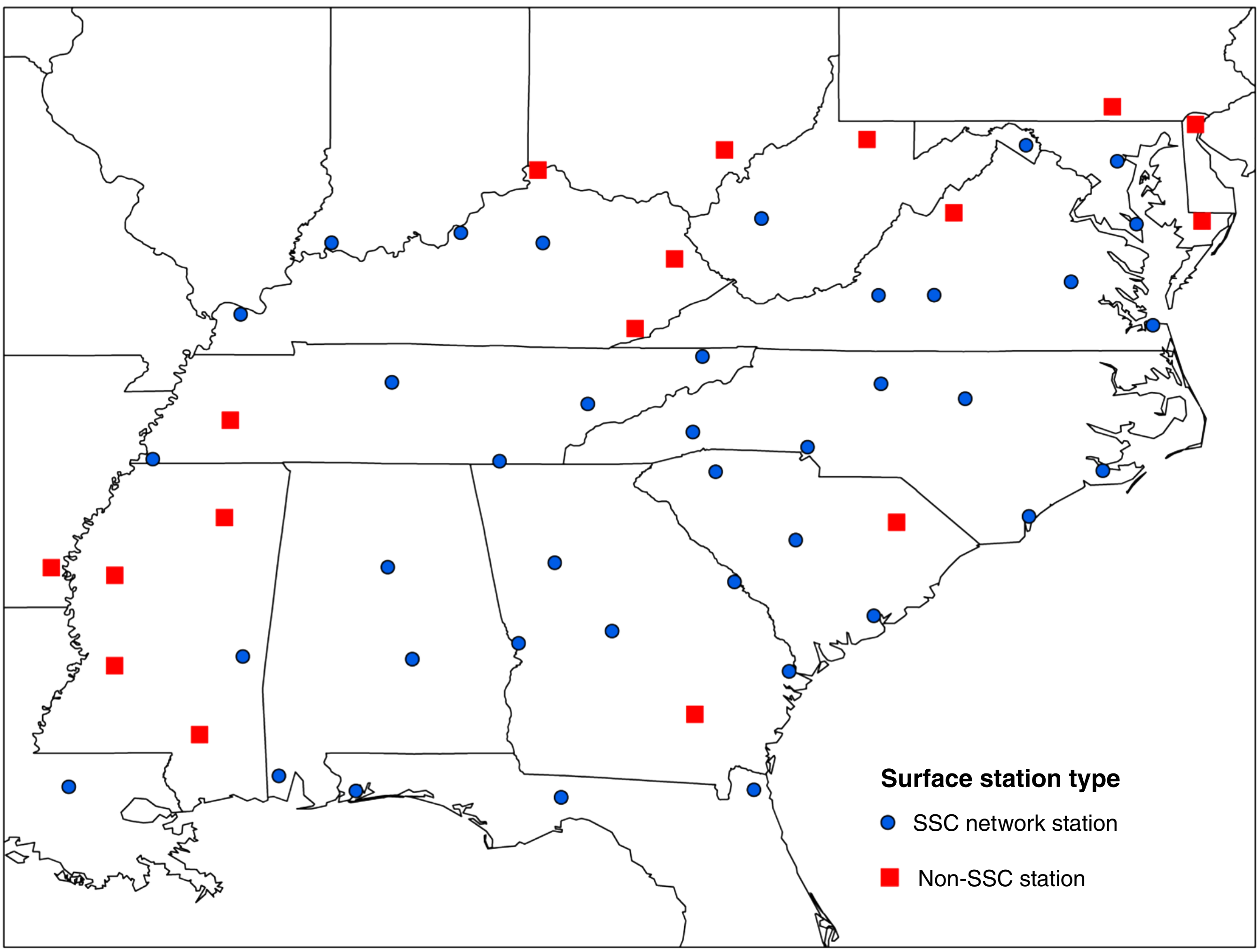

FIGURE 3 Map of surface stations [Colour figure can be viewed at wileyonlinelibrary.com]

(both tropical or transitioning extratropical systems), or a combination of these. The combination category was included to eliminate problems of subjectivity for events in which there were two or more surface forcings present. This allowed for further explanation of the SSC classification for the most intense IPEs by identifying the type of forcing mechanism associated with the IPEs and SSC weather types.

3 | RESULTS

3.1 | IPE trends

3.1.1 | Annual frequency and intensity of IPE

The total number of IPEs identified for the study area was 7,704. Across the entire study area, IPEs showed statistically significant increasing trends in frequency (p = .013), adjusted event strength (p = .005), and amount of precipitation per IPE (p = .008) (Figure 4 and Table 1). Generally, stations with increasing polewards latitude from the Gulf of Mexico, westwards inland locations from the Atlantic Coast, and stations at higher elevations had lower adjusted IPE strength thresholds (see Figure 2).

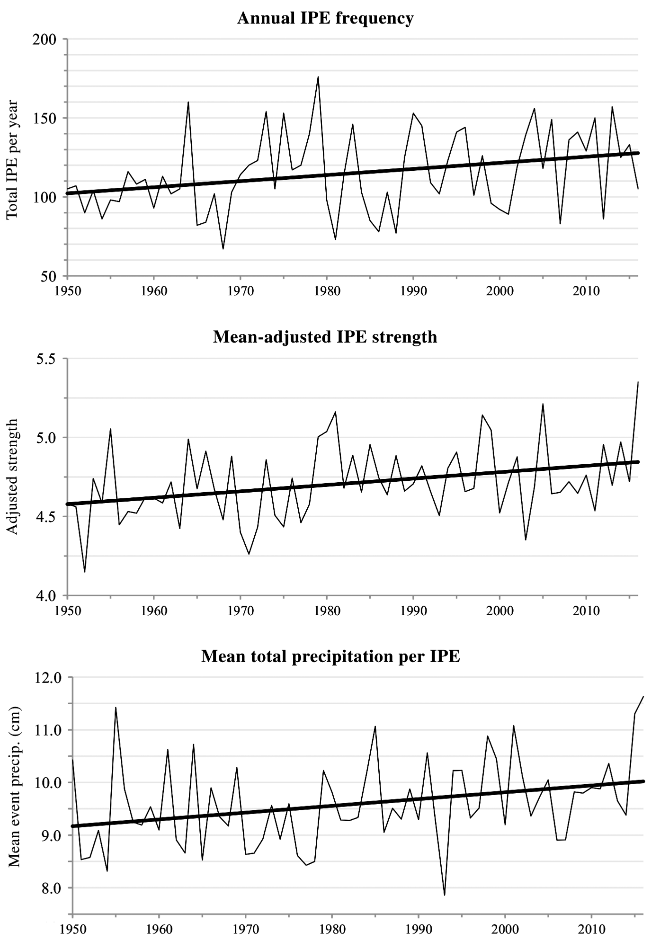

FIGURE 4 (top) Annual IPE frequency; (middle) annual mean adjusted IPE strength; (bottom) annual mean total precipitation per IPE. Trend statistics can be found in Table 1

Despite the significant results, many r^2 values in the results are low. Practical significance can be gauged by the linear change in the average number of IPEs from 1950 to 2016, or the percent change in strength. The number of annual IPEs increased at a linear rate of 0.38 events per year since 1950, and the average amount of precipitation per IPE increased linearly by 0.85 cm from 1950 to 2016. Annual trends for the SeUS in Mallakpour and Villarini (2017) using a 95th percentile "peaks over threshold" method, showed that 19.3% of the pixel area of the region has experienced significant increases in extreme precipitation.

As was discussed by Krichak *et al*. (2014) and Mallakpour and Villarini (2017), the phases of certain teleconnections play an important role in annual variability of IPE recurrence. When analysing Figure 4, the inter-annual variability for IPE frequency was small from 1950 to 1963; however, 1963–2016 was marked by larger variance in the total number of IPEs, as well as a sharper increasing trend in variance. El Niño–Southern Oscillation (ENSO), the North Atlantic Oscillation (NAO), and the Atlantic Multidecadal Oscillation (AMO) are three primary teleconnections responsible for seasonal and inter-annual hydroclimatic variability in the SeUS (Labosier and Quiring, 2013; Engström and Waylen, 2018). Pearson correlations between the annual and seasonal numbers of IPEs and ENSO, NAO, and AMO were performed to help explain the IPE variance. Only El Niño, using the winter season (NDJFM) Niño3.4 region sea surface temperatures (National Oceanic and Atmospheric Administration Earth Systems Research Laboratory, 2018), was significant with IPEs in these months across the SeUS (r = 0.28, p = .02). El Niño is associated with a greater number of mid-latitude and extratropical storm tracks across the SeUS during the winter months (Curtis, 2006; Senkbeil *et al*., 2011). The three strongest El Niño seasons (1982–1983, 1997–1998, 2015–2016) were ranked eighth, third, and ninth in the number of IPEs across the region. Other subregional teleconnection results are shared in later sections.

Variability in the position and orientation of the subtropical high also influences the variability of IPEs, primarily in the warm season months for the SeUS (Li *et al*., 2011; Labosier and Quiring, 2013). The subtropical high's position and orientation also contributes to inter-annual variance in the United States hurricane landfalls, which are a major IPE producer. Average tropical cyclone rainfall rates are projected to increase in future climate modelling scenarios in the region (Wright *et al*., 2015).

While teleconnection phases, atmospheric circulation anomalies, and tropical cyclone landfalls are potential explanations for observed annual variability, these do not entirely explain the statistically significant increase in the total number of annual IPEs. Emori and Brown (2005) assert that increases in atmospheric vertical motion and moisture are expected to lead to increased recurrence of IPEs, with

TABLE 1 (top) 1950–2016 IPE trend statistics for the entire study area. (middle) Latitude and (bottom) physiographic subregion IPE trend statistics. Bold is significant at an alpha level of 0.05

Full study area trends	Annual IPE frequency *p*	r^2	Change
Annual IPE frequency	**.013**	**0.09**	**+25.50**
Mean-adjusted IPE strength	**.005**	**0.12**	**+5.87%**
Mean total precipitation per IPE	**.008**	**0.10**	**+0.85 cm**

	Annual IPE frequency			IPE-adjusted strength		
Latitudinal region	*p*	r^2	Change	*p*	r^2	Percent change
North	**.049**	**0.06**	**+5.947**	0.389	0.01	2.8
North Central	**.031**	**0.07**	**+6.574**	0.078	0.05	6.2
Central	0.079	0.05	+5.452	0.626	0.01	1.5
South Central	0.301	0.02	+2.996	0.077	0.05	5.8
South	0.143	0.03	+4.534	0.058	0.05	7.6

	Annual IPE frequency			IPE-adjusted strength		
Physiographic region	*p*	r^2	Change	*p*	r^2	Percent change
Atlantic Coastal Plain	.757	0.00	+1.069	**0.016**	**0.09**	**8.0**
Piedmont	.080	0.05	+3.993	0.479	0.01	4.3
Appalachian Highlands	.066	0.04	+6.131	0.377	0.01	−2.5
Ohio–Mississippi Valley	**.011**	**0.10**	**+7.135**	0.090	0.04	6.1
Gulf Coastal Plain	**.028**	**0.07**	**+7.187**	0.106	0.04	5.1

changes in atmospheric moisture being the more important of these two factors in the SeUS. Both the frequency and intensity of IPEs have significantly increased in the region suggesting that, in addition to increasing atmospheric moisture content, the forcing mechanisms responsible for IPEs are possibly becoming more common, more volatile, or perhaps characterized by greater longevity. With statistically significant increasing trends in both the annual total and average strength of IPEs, questions arise about what subregions within the study area have contributed the most to the significance of these trends. The following sections use the previously discussed subregions (see Figure 1) to identify the areas of the SeUS that are responsible for the bulk of the IPE frequency and intensity trend significance.

3.1.2 | Subregional frequency and intensity of IPE

All latitudinally derived subregions within the SeUS have experienced at least a slight increase in the total number of IPEs per year on average. This increase is statistically significant for both the North ($p = .049$) and the North Central ($p = .031$) regions, but was not significant in the three southern regions (Figure 5 and Table 1). These results are meaningful in that they imply that as one progresses farther northwards, a more marked increase in the total number of annual IPEs can be expected. Similarly, the North and North Central regions in this research match the increasing frequency trends for these approximate latitudes in Mallakpour and Villarini (2017). No individual region appears to have experienced markedly higher variability than the others across all latitudes in the SeUS. An explanation for increasing IPE with latitude is possibly due to changes in surface weather type frequency, which is discussed in later sections.

El Niño showed statistically significant positive relationships with IPEs during the winter months across the South Central ($r = 0.39$, $p < .01$) and South ($r = 0.27$, $p = .03$) latitude regions, which confirms results of previous research (Curtis, 2006; Senkbeil *et al*., 2011). Positive NAO was statistically significant in the North Central region during winter ($r = 0.26$, $p = .04$).

Similar to the latitudinal results, Figure 6 shows that all physiographic provinces except for the Atlantic Coastal Plain ($p = .757$) have experienced slight increases in the frequency of IPEs per year. This lack of a trend in the Atlantic Coastal Plain can likely be attributed to its proximity to the Atlantic Ocean and influences from large-scale teleconnections (Tootle *et al*., 2005; Mallakpour and Villarini, 2017). Specifically, inter-annual variability in the Bermuda high (Diem, 2013; Powell and Keim, 2015) impacts synoptic-scale annual and seasonal trends and can alter the path of tropical cyclones closer to or farther from the coastline. The Atlantic Coastal Plain has experienced a statistically significant increase in IPEs during the winter months for El Niño events ($r = 0.45$, $p < .01$). This suggests that non-El Niño years are characterized by fewer IPEs in this subregion, unless that is offset by an active tropical season.

The Ohio–Mississippi Valley ($p = .011$), and Gulf Coastal Plain ($p = .028$) regions experienced statistically significant increases in the total number of IPEs per year (Table 1). This result appears to indicate that areas to the west and to the south of the Appalachians have experienced a more significant increase in the total number of IPEs than areas within or to the east of the Appalachian Mountains. The Ohio–Mississippi Valley subregion had a statistically significant negative relationship with El Niño ($r = -0.27$,

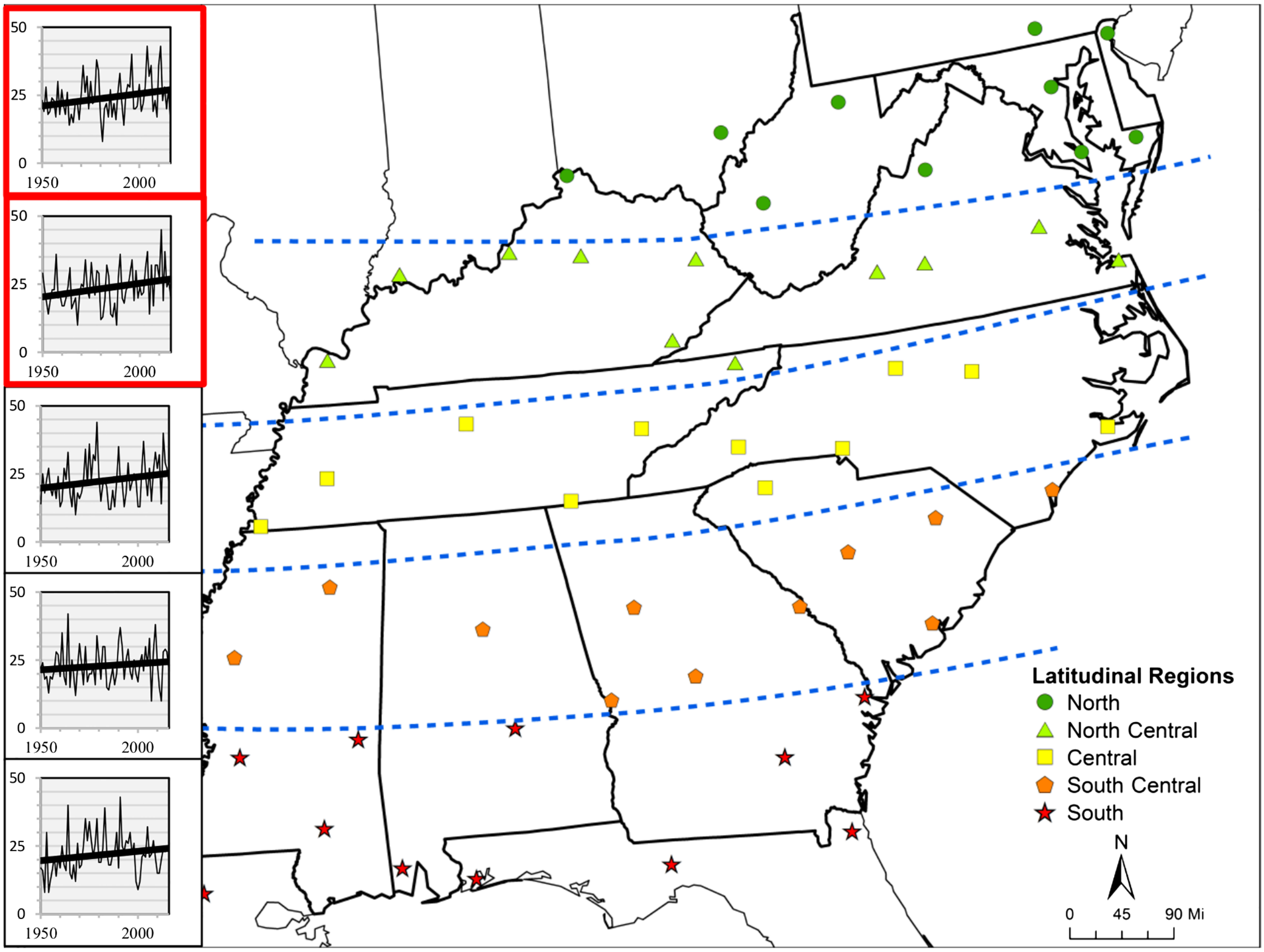

FIGURE 5 Latitudinal subregion trends in total number of IPEs per year. Each linear trend graph top to bottom corresponds with the north to south latitude subregion. Graphs that display statistical significance are shown with a thick outline. Trend statistics can be found in Table 1

$p = .03$), while also displaying a similar NAO result ($r = 0.36$, $p < .01$) in comparison to the North Central latitude subregion. The Appalachian Highland region ($p = .066$) has also experienced large annual variability similar to that of the Atlantic Coastal Plain (Table 1). The Atlantic Coastal Plain was the only subregion that did not contribute to the increase in the total number of annual IPEs, a result that contrasts somewhat with Mallakpour and Villarini (2017).

The physiographic results appear to juxtapose the latitudinal region results, in that the southernmost latitudinal subregion did not experience statistically significant change, but physiographically there is significant change in the Gulf Coastal Plain. This juxtaposition is driven principally by these two subregions not sharing many of the same stations, with the southern latitudinal region containing multiple stations win the Atlantic Coastal Plain, which has not experienced an increase in IPE frequency. Physiographic and latitudinal results for IPE intensity were not as strong as the results for frequency, with only the Atlantic Coastal Plain ($p = .016$) showing a significant increase in adjusted IPE strength. As such, no figures were included for subregional IPE adjusted strength, but trend statistics were included, and can be seen in Table 1.

3.1.3 | Seasonal frequency of IPE

Along with determining whether IPEs have become more common or stronger over time, an important goal of this research is to identify the seasonality of IPEs, both across the entire study area and the different subregions. The monthly and seasonal distribution of IPEs across the entire study area is displayed in Table 2. There are distinct peaks during both TR seasons when contrasting air masses collide more often, and a steady peak in the summer months when there is ample convective energy available. September had the greatest monthly total, likely due to tropical forcings with some extratropical inputs in the more northern latitudes.

In addition to the utility of knowing the seasonal distribution of IPEs through the entire study period, it is also important to know if the seasonality of IPEs has changed over time. Every season has experienced an increase in the total number of IPEs per year, but fall (September, October, November) is the only season that has experienced a

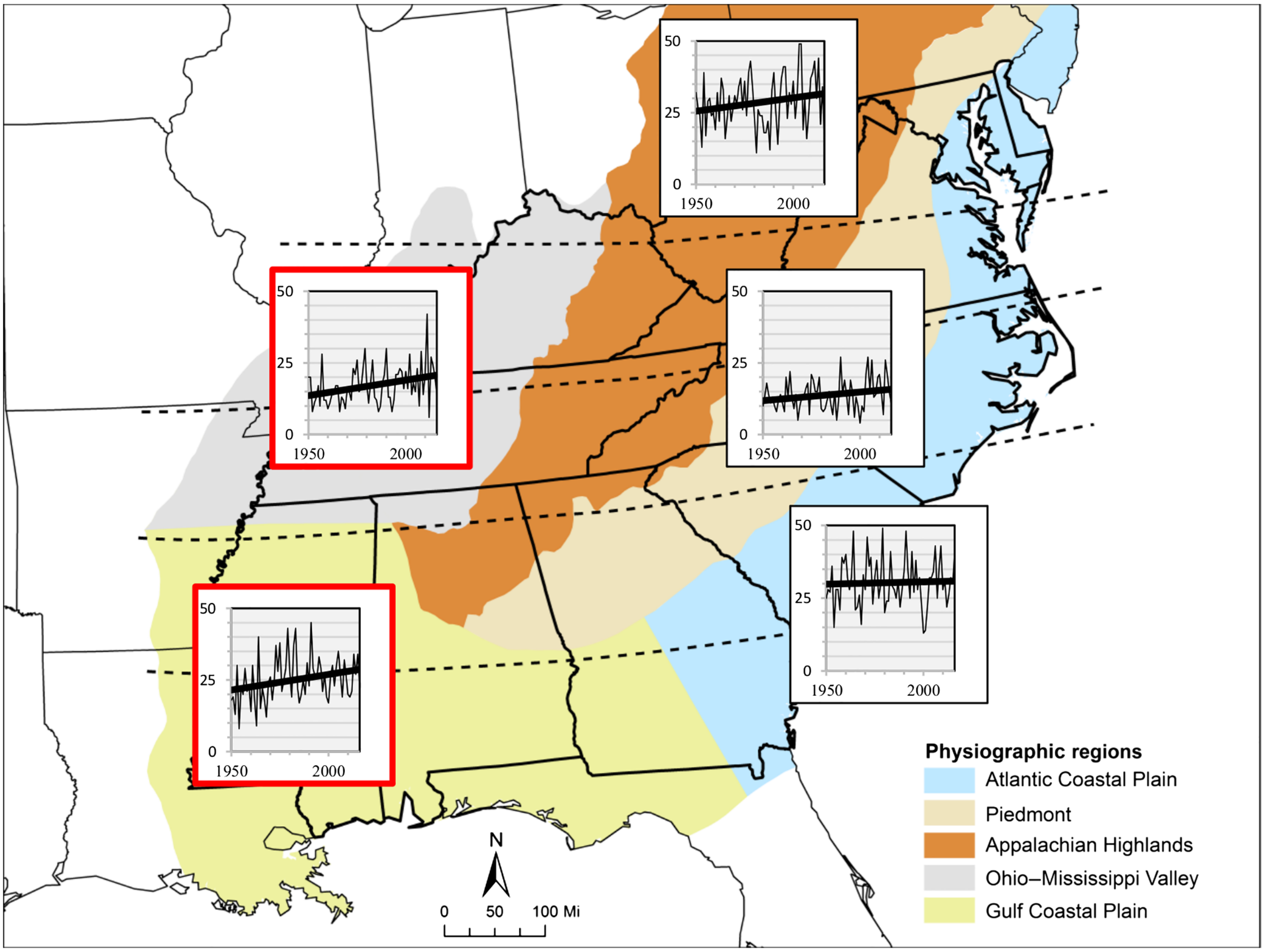

FIGURE 6 Physiographic subregion trends in total number of IPEs per year. Each linear trend graph is overlain onto its corresponding physiographic subregion. Graphs that display statistical significance are shown with a thick outline. Trend statistics can be found in Table 1 [Colour figure can be viewed at wileyonlinelibrary.com]

statistically significant increase in IPEs (p = .038). This result was also confirmed by Mallakpour and Villarini (2017), with 17.9% of their grid cells in the southeastern region showing a significant fall increase in magnitude and 20.6% for frequency. An explanation for the fall increase in IPEs in the SeUS is attributed to tropical influences from more landfalling storms, especially during the positive phase of the AMO starting in 1995 (Nogueira and Keim, 2010). Many of these landfalls were characterized by slower moving storms, or storms with expanding westwards precipitation swaths during extratropical transition, which became inland IPEs within the region (Zhou and Matyas, 2017).

3.2 | SSC IPE trends and surface forcing mechanisms

One of the goals of using the SSC in this research was to see if any of the SSC weather types have become more or less common with IPEs over time. Evidence of shifting weather types could indicate changing surface conditions as they relate to IPEs. Each IPE was assigned an SSC surface weather type classification. Of the 7,704 IPEs, 24 were not assigned an SSC classification due to incomplete data for the day in question, resulting in a total of 7,680 total IPEs. The distribution of SSC weather types associated with IPEs shows the prevalence of the MM weather type with 44% of the total IPEs, followed by TR at 27%, MT at 20%, and MP at 9% (Table 3). MM and MT days when IPEs occurred were most common in summer, TR days were most common in fall and spring, and MP days were more likely to occur in spring, fall, or winter (see Table 3). Each season's distributions of SSC weather types can be seen in Table 3 as well. Fall and winter IPEs were dominated by TR and MM weather types, while spring and summer IPEs were most commonly associated with MM weather types, with secondary dependence on TR weather types in spring, and MT weather types in summer.

A closer regional examination of IPEs and the surface forcing mechanisms associated with each weather type provided a better explanation for the types of weather patterns responsible for IPEs. Of the 150 most intense IPEs (30 per physiographic subregion), 75 were associated with MM days. This was more typical across the northern latitudes of

TABLE 2 (top) Monthly IPE distribution; (bottom) seasonal IPE trend statistics 1950–2016. Bold is significant at an alpha level of 0.05

	Monthly IPE distribution	
Month	**Total IPE**	**Percent contribution**
Jan	384	5.0
Feb	394	5.1
Mar	693	9.0
Apr	574	7.5
May	604	7.8
Jun	670	8.7
Jul	911	11.8
Aug	863	11.2
Sep	973	12.6
Oct	602	7.8
Nov	510	6.6
Dec	526	6.8
Total	7,704	

	IPE 1950–2016		
Season	***p***	**r^2**	**Increase**
Winter	.228	0.02	4.686
Spring	.292	0.02	4.877
Summer	.171	0.03	5.405
Fall	**.038**	**0.06**	**10.540**

the study area where an MT weather type was modified under thicker cloud cover or modified by the influence of a mid-latitude weather system, thus reducing the temperature of the original MT weather type. This is substantiated by the distribution of surface forcing mechanisms for MM days. Of the 75 MM days, 21 were tropical systems, 20 were stationary fronts, and an additional 21 were either non-tropical low-pressure systems or cold fronts (Table 4). The stationary fronts were spread more evenly throughout the year, while the non-tropical lows and cold fronts were concentrated in the TR season months. Furthermore, the mean length of an MM IPE was 2.73 days. Although the frequency of IPEs has not increased for MM days (see Table 5), it remains the strongest contributor of any weather type to total amounts of precipitation.

TABLE 4 SSC weather type and surface forcing mechanisms for the top 30 most intense IPE in each physiographic subregion. Bold indicates the dominant SSC class associated with each surface forcing mechanism

		SSC weather type			
Surface forcing	**Total**	**MP**	**MM**	**MT**	**TR**
Air mass	7	0	**4**	2	1
Cold front	14	0	**7**	2	5
Combination	14	0	**9**	2	3
Low pressure	29	2	**14**	4	9
Stationary	32	3	**20**	7	2
Tropical	54	1	21	1	**31**
Total	150	6	**75**	18	51

TABLE 5 (top) 1950–2016 IPE trend statistics for each SSC weather type; (middle) latitude and (bottom) physiographic subregion MT IPE trend statistics 1950–2016. Bold is significant at an alpha level of 0.05

	Annual IPE frequency		
SSC classification	***p***	**r^2**	**Increase**
MP	.811	0.001	0.49
MM	.71	0.002	2.10
MT	**<.01**	**0.222**	**12.53**
TR	.078	0.047	8.40
	MT IPE frequency		
Latitudinal region	***p***	**r^2**	**Increase**
North	.181	0.023	1.29
North Central	**<.01**	**0.161**	**3.51**
Central	**<.01**	**0.101**	**3.07**
South Central	.08	0.044	2.11
South	**.011**	**0.096**	**2.55**
	MT IPE frequency		
Physiographic region	***p***	**r^2**	**Increase**
Atlantic Coastal Plain	.09	0.041	1.72
Piedmont	**<.01**	**0.247**	**2.98**
Appalachian Highlands	.102	0.038	1.94
Ohio–Mississippi Valley	**.02**	**0.071**	**2.23**
Gulf Coastal Plain	**<.01**	**0.119**	**3.67**

The other weather types had a more dominant forcing mechanism. IPEs on TR days had a nearly significant

TABLE 3 (top) Percent seasonal distribution of each SSC weather type, and (bottom) percentage of each season's IPEs produced by each SSC weather type

	Seasonal percentage SSC contribution					
Weather type	**Winter (%)**	**Spring (%)**	**Summer (%)**	**Fall (%)**		**Total (%)**
MP	23.7	29.7	17.0	29.6	100%	653 (9)
MM	11.0	23.0	39.6	26.4	100%	3,402 (44)
MT	19.1	23.0	40.9	17.0	100%	1,532 (20)
TR	23.1	25.4	16.7	34.8	100%	2,093 (27)

	SSC percentage seasonal contribution			
Weather type	**Winter (%)**	**Spring (%)**	**Summer (%)**	**Fall (%)**
MP	11.9	10.4	4.6	9.3
MM	28.7	42.1	55.4	43.2
MT	22.4	19.0	25.7	12.5
TR	37.0	28.6	14.3	35.0
	100	100	100	100
Total (%)	1,304 (17)	1,862 (24)	2,433 (32)	2,081 (27)

increase across the study area ($p = .08$) (Table 5). Of the 51 IPE TR days analysed on surface maps, 31 are associated with a tropical system, which explains the seasonal fall occurrence when many tropical systems make landfall in September or early October. Non-tropical lows and cold fronts combine to comprise 14 TR days, primarily in the cool season months (see Table 4).

IPE MT days showed a statistically significant increase ($p < .01$) with a linear increase from approximately 17 per year in 1950, to 29 per year in 2016 (Table 5). There was less variance with MT than many of the previously discussed annual trends. An increase in annual MT IPEs may be due to more common northwards and inland encroachment of MT air over time. A summer increase and northwards encroachment of summer MT frequency was identified by Senkbeil *et al.* (2017) in eastern North America, but the IPE MT days in this research occurred most often in the summer months, peaking in July. IPE MT days were distributed across all forcing mechanisms, but stationary fronts were the most common, followed by non-tropical lows. Further reinforcing this result was Collow *et al.* (2016), who found that extreme precipitation events associated with cut-off lows were becoming more common in the northeast United States air mass thunderstorm IPEs were uncommon with MT since these events are sporadic in coverage and also normally brief in duration. MP days were rare but often times involved a stationary front or non-tropical low. One MP event was the result of a tropical system in the Piedmont region when Hurricane Flossy (1956) ingested polar air from Canada during its extratropical transition.

3.2.1 | MT subregions

To explore further Senkbeil *et al.*'s (2017) finding evidence of increasing summer MT frequency by latitude, MT was also partitioned by latitude in this research since it was the only weather type to show a significantly increasing IPE trend. Three subregions have exhibited statistically significant increases in the frequency of MT (Figure 7). The North Central region ($p < .01$) has experienced the most significant increase in total MT IPEs, while the Central ($p < .01$) and Southern ($p = .01$) regions have all experienced significant increases in MT

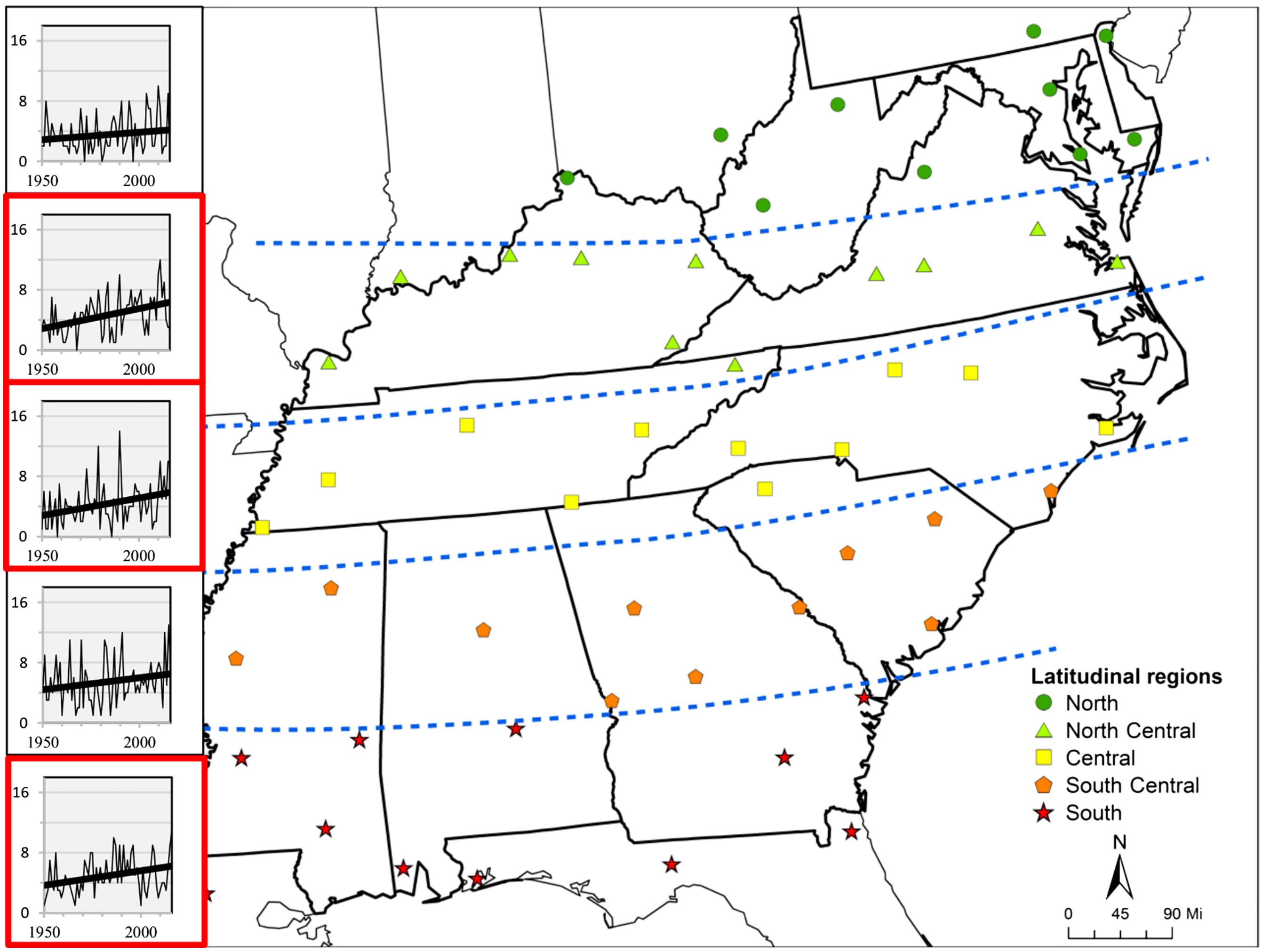

FIGURE 7 Latitudinal subregion trends in total number of MT IPEs per year. Each linear trend graph top to bottom corresponds with the north to south latitude subregion. Graphs that display statistical significance are shown with a thick outline. Trend statistics can be found in Table 5 [Colour figure can be viewed at wileyonlinelibrary.com]

IPEs. Despite the fact that the northernmost latitudinal region has not experienced a significant increase ($p = .181$), these results appear to confirm the hypothesis that the significant increase in the total number of MT IPEs per year can be attributed to more common northwards encroachment of warm and moist weather types over time, especially in the months between May and September.

Physiographically, three subregions were found to be displaying significant increases. The Gulf Coastal Plain ($p = .004$), Piedmont ($p < .01$), and Ohio–Mississippi Valley ($p = .020$) regions have all displayed statistically significant increases in the total number of MT IPEs per year (Figure 8). Particularly the increases in the Piedmont and Ohio–Mississippi Valley regions appear to confirm the hypothesis that MT weather types, along with encroaching northwards more often, are also encroaching inland more often; however, the lack of significance and increasing annual variability in the Appalachians ($p = .102$) shows that the increase has not occurred consistently in mountainous areas, largely due to orographic influences on temperature.

4 | CONCLUSION

In this research, spatial and temporal changes in IPEs were evaluated for the SeUS from 1950 to 2016 using 56 surface stations. Trends were assessed annually and seasonally across the entire study area, and spatially by partitioning stations into latitude and physiographic subregions. Additionally, surface weather type trends and a smaller subset of associated surface forcing mechanisms were evaluated to determine the surface weather conditions that were the most common contributors to IPEs.

Results revealed that annual IPE frequency and magnitude (which is adjusted by event length and intensity) both significantly increased over time. These results were also found by Mallakpour and Villarini (2017), with a gridded pixel analysis approach, albeit with a greater number of significant results for frequency compared to precipitation magnitude. Fall was the only season to show a significant increasing IPE trend, which was also identified by Mallakpour and Villarini (2017), particularly in a swath from Tennessee to Louisiana.

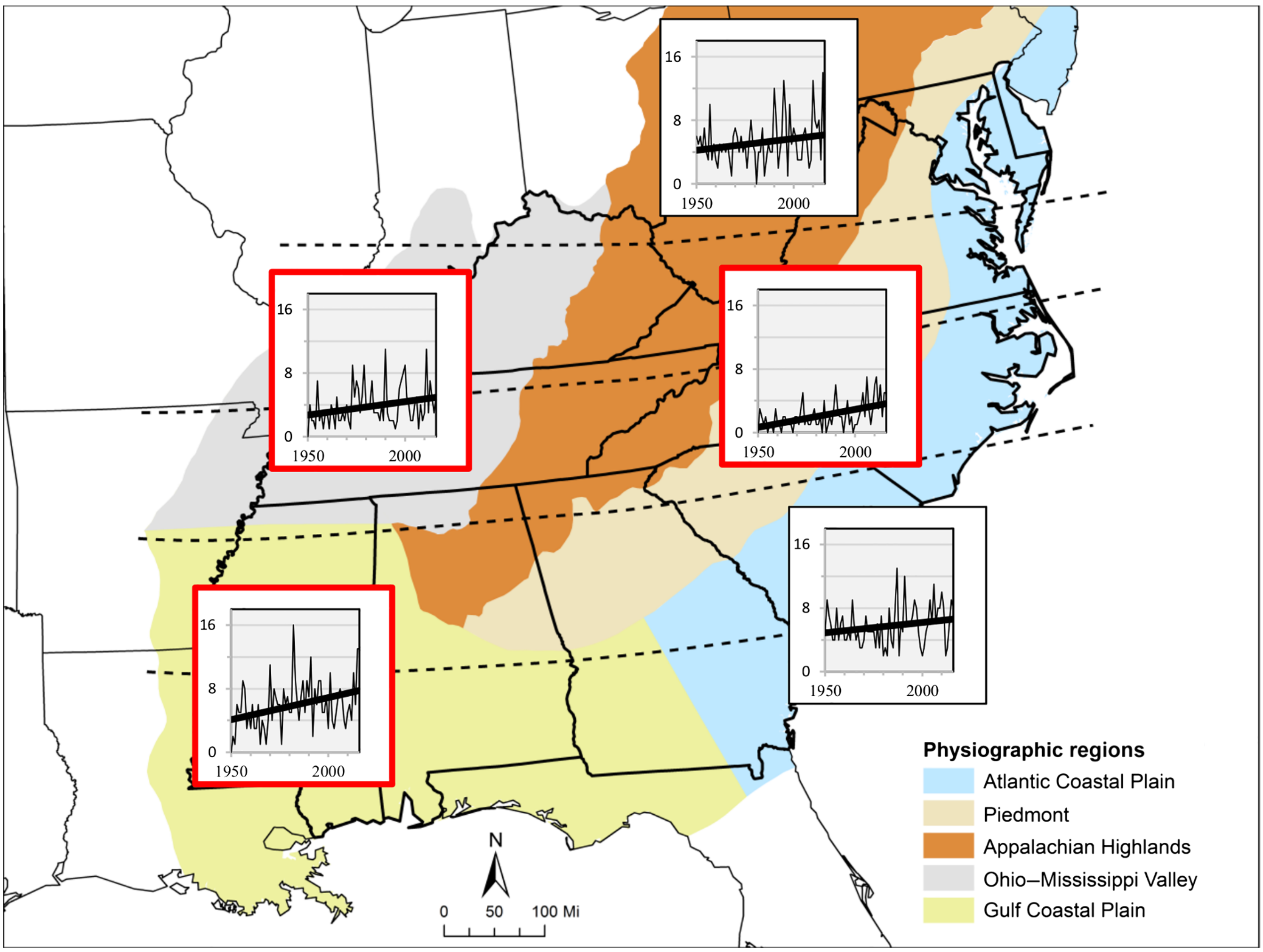

FIGURE 8 Physiographic subregion trends in total number of MT IPEs per year. Each linear trend graph is overlain onto its corresponding physiographic subregion. Graphs that display statistical significance are shown with a thick outline. Trend statistics can be found in Table 5 [Colour figure can be viewed at wileyonlinelibrary.com]

Dividing the study area into latitude subregions of equal sample sizes revealed that most stations in the North and North Central subregions have shown the greatest increases in IPE frequency. These results align fairly well with Mallakpour and Villarini (2017) who displayed a high concentration of grid cells at these latitudes with increasing frequency, and also along the Gulf Coastal states south between approximately 33 and 30°N latitude. The concentration in these two areas of the study region also aligns well with significant physiographic subregion results across the Ohio–Mississippi Valley and the Gulf Coastal Plain.

Use of the SSC as a surface weather typing scheme, revealed that the MT weather type was associated with significant annual IPE increases. Latitude subregions with the greatest increases in annual MT IPEs were found in the South, Central, and North Central subregions primarily between May and September when MT has been significantly increasing (Senkbeil *et al*., 2017); however, MT IPEs represent only 20% of all IPE days. Although the MM weather type has been the most common IPE-producing weather type, MM IPE days have not significantly increased. The most common surface forcing mechanisms associated with IPEs ranked in order are tropical events that are commonly transitioning into extratropical lows, stationary fronts, and non-tropical low-pressure systems.

Teleconnections such as ENSO, NAO, and AMO have well-documented relationships with seasonal and annual precipitation increases and decreases across the SeUS. Results from this research largely confirm the results of previous precipitation research regarding ENSO and NAO, although AMO was not significant with IPEs. Teleconnections play an exacerbating role in the increase of IPEs, but fail to fully explain the reasons for increases in IPE frequency and magnitude. The finding of more IPEs on MT days is also an ancillary explanation for the increasing IPE results since MT are only 20% of the IPE days. Furthermore, there has not been a significant increase in the frequency of landfalling tropical cyclones in the United States (Vecchi and Knutson, 2011), which detracts from speculation that a tropical signal is responsible for the IPE increase. The exact explanations for the results in this research are unknown. Both natural climatic variability and climate change are reasons for the uncertainty in future climate modelling projections, but at the regional-scale climate change can be more reliably detected for extreme precipitation (Martel *et al*., 2018). Climate change is hypothesized to be the most viable interpretation for the results in this research, despite the lack of a uniform temperature increase across the SeUS.

Increased frequency of IPEs is a climatological occurrence that calls for careful planning and management of water resources in the present and in the future. The SeUS is a region where IPEs are becoming more common and more intense, leading to possible increases in water surplus. Certain surface weather conditions are more favourable for the development of IPEs, and these conditions can be forecast with enough lead-time to properly plan for the harmful and beneficial impacts. Future research will employ modelling scenarios to estimate the projected likelihood of IPEs, while incorporating the uncertainty of climate model projections. Additionally, future research will evaluate the upper atmospheric characteristics of large spatial-scale IPEs, to better understand the atmospheric flow patterns associated with the most intense IPEs.

ORCID

Walker J. Skeeter http://orcid.org/0000-0003-3088-812X

REFERENCES

Agel, L., Barlow, M., Qian, J-H, Colby, F., Douglas, E, & Eichler, T. (2015) Climatology of daily precipitation and extreme precipitation events in the Northeast United States. *Journal of Hydrometeorology*, 2537-2557. https://doi.org/https://doi.org/10.1175/JHM-D-14-0147.1.

Allen, M. and Sheridan, S. (2016) Spatio-temporal changes in heat waves and cold spells: an analysis of 55 U.S. cities. *Physical Geography*, 37, 189–209. https://doi.org/10.1080/02723646.2016.1184078.

Anderegg, W.R., Kane, J. and Anderegg, L. (2013) Consequences of widespread tree mortality triggered by drought and temperature stress. *Nature Climate Change*, 3, 30–36. https://doi.org/10.1038/NCLIMATE1635.

Ashley, W., Bentley, M. and Stallins, J. (2012) Urban-induced thunderstorm modification in the southeast United States. *Climatic Change*, 113, 481–498. https://doi.org/10.1007/s10584-011-0324-1.

Barros, A., Hodes, J. and Arulraj, M. (2017) Decadal climate variability and the spatial organization of deep hydrological drought. *Environmental Research Letters*, 12, 1–12. https://doi.org/10.1088/1748-9326/aa81de.

Bentley, M., Stallins, A. and Ashley, W. (2012) Short communication: synoptic environments favourable for urban convection in Atlanta, Georgia. *International Journal of Climatology*, 32, 1288–1294. https://doi.org/10.1002/joc.2344.

Berghuijs, W., Aalbers, E., Larsen, J., Trancoso, R. and Woods, R. (2017) Recent changes in extreme floods across multiple continents. *Environmental Research Letters*, 12, 1–7. https://doi.org/10.1088/1748-9326/aa8847.

Brody, S.D., Highfield, W.E. and Kang, J.E. (2011) *Rising Waters: The Causes and Consequences of Flooding in the United States*. Cambridge: Cambridge University Press.

Chou, C., Chen, C.-A., Tan, P.-H. and Chan, K.T. (2012) Mechanisms for global warming impacts on precipitation frequency and intensity. *Journal of Climate*, 25, 3291–3306. https://doi.org/10.1175/JCLI-D-11-00239.1.

Collow, A., Bosilovich, M. and Koster, R. (2016) Large-scale influences on summertime extreme precipitation in the northeastern United States. *Journal of Hydrometeorology*, 17, 3045–3061. https://doi.org/10.1175/JHM-D-16-0091.1.

Curtis, S. (2006) Developing climatology of the south's "other" storm season ENSO impacts on winter extratropical cyclogenesis. *Southeastern Geographer*, 46, 231–244.

Diem, J.E. (2013) Influences of the Bermuda high and atmospheric moistening on changes in summer rainfall in the Atlanta, Georgia region, USA. *International Journal of Climatology*, 33, 160–172. https://doi.org/10.1002/joc.3421.

Dixon, G. and Mote, T. (2003) Patterns and causes of Atlanta's urban heat Island-initiated precipitation. *Journal of Applied Meteorology*, 42, 1273–1284. https://doi.org/10.1175/1520-0450(2003)042<1273:PACOAU>2.0.CO;2.

Emori, S. and Brown, S.J. (2005) Dynamic and thermodynamic changes in mean and extreme precipitation under changed climate. *Geophysical Research Letters*, 32, 1–5. https://doi.org/10.1029/2005GL023272.

Engström, J. and Waylen, P. (2018) Drivers of long-term precipitation and runoff variability in the southeastern USA. *Theoretical and Applied Climatology*, 131, 1133–1146. https://doi.org/10.1007/s00704-016-2030-4.

Fenneman, N. and Johnson, D. (1946) *Physiographic divisions of the conterminous U.S.* Reston, VA: U.S. Geological Survey.

Fischer, E.M. and Knutti, R. (2016) Anthropogenic contribution to global occurrence of heavy-precipitation and high-temperature extremes. *Nature Climate Change*, 5, 560–564. https://doi.org/10.1038/NCLIMATE2617.

Frich, P., Alexander, L.V., Della-Marta, P., Gleason, B., Haylock, M., Tank Klein, A. and Peterson, T. (2002) Observed coherent changes in climatic extremes during the second half of the twentieth century. *Climate Research*, 19, 193–212. https://doi.org/10.3354/cr019193.

Grose, M.R., Risbey, J.S. and Whetton, P.H. (2017) Tracking regional temperature projections from the early 1990s in light of variations in regional warming, including "warming holes". *Climatic Change*, 140, 307–322. https://doi.org/10.1007/s10584-016-1840-9.

IPCC. (2013) Near term climate change: projections and predictability. In: *Climate Change: The Physical Science Basis*, Cambridge, UK: Cambridge University Press, pp. 953–1028.

Janssen, E., Wuebbles, K. and Kunkel, K. (2014) Observational and model based trends and projections of extreme precipitation over the contiguous United States. *Earth's Future*, 2, 1–15. https://doi.org/10.1002/2013EF000185.

Jones, J., Schwartz, J., Ellis, K., Hathaway, J. and Jawdy, C. (2015) Temporal variability of precipitation in the upper Tennessee Valley. *Journal of Hydrology: Regional Studies*, 3, 2261–2272. https://doi.org/10.1016/j.ejrh.2014.10.006.

Keim, B.D. (1996) Spatial, synoptic, and seasonal patterns of heavy rainfall in the southeastern United States. *Physical Geography*, 17, 313–328.

Keim, B.D. (1997) Preliminary analysis of the temporal patterns of heavy rainfall across the southeastern United States. *The Professional Geographer*, 49, 94–104. https://doi.org/10.1111/0033-0124.00060.

Krichak, S.O., Breitgand, J., Gualdi, S. and Feldstein, S. (2014) Teleconnection–extreme precipitation relationships over the Mediterranean region. *Theoretical and Applied Climatology*, 117, 679–692. https://doi.org/10.1007/s00704-013-1036-4.

Kunkel, K.E., Easterling, D., Kristovich, D., Gleason, B., Stoecker, L. and Smith, R. (2012) Meteorological causes of the secular variations in observed extreme precipitation events for the conterminous United States. *Journal of Hydrometeorology*, 13, 1131–1141. https://doi.org/10.1175/JHM-D-11-0108.1.

Labosier, C. and Quiring, S. (2013) Hydroclimatology of the southeastern USA. *Climate Research*, 57, 157–171. https://doi.org/10.3354/cr01166.

Li, W., Li, L., Fu, R., Deng, Y. and Wang, H. (2011) Changes to the North Atlantic subtropical high and its role in the intensification of summer rainfall variability in the southeastern United States. *Journal of Climate*, 24, 1499–1506. https://doi.org/10.1175/2010JCLI3829.1.

Mallakpour, I. and Villarini, G. (2017) Analysis of changes in the magnitude, frequency, and seasonality of heavy precipitation over the contiguous USA. *Theoretical and Applied Climatology*, 130, 345–362. https://doi.org/10.1007/s00704-016-1881-z.

Martel, J.-L., Mailhot, A., Brissette, F., & Caya, D. (2018) Role of natural climate variability in the detection of anthropogenic climate change signal for mean and extreme precipitation at local and regional scales. *Journal of Climate*, 4241-4263. https://doi.org/https://doi.org/10.1175/JCLI-D-17-0282.1.

McGuire, B. (2010) Potential for a hazardous geospheric response to projected future climate changes. *Philosophical Transactions of the Royal Society A*, 368, 2317–2345. https://doi.org/10.1098/rsta.2010.0080.

Meehl, G.A., Arblaster, J.M. and Chung, C.T.Y. (2015) Disappearance of the southeast U.S. "warming hole" with the late 1990s transition of the Interdecadal Pacific Oscillation. *Geophysical Research Letters*, 42, 5564–5570. https://doi.org/10.1002/2015GL064586.

Moore, B.J., Mahoney, K., Sukovick, E., Cifelli, R. and Hamill, T. (2015) Climatology and environmental characteristics of extreme precipitation events in the southeastern United States. *Monthly Weather Review*, 143, 718–741. https://doi.org/10.1175/MWR-D-14-00065.1.

National Oceanic and Atmospheric Administration Earth Systems Research Laboratory. (2018) El Nino Southern Oscillation (ENSO). Available at: https://www.esrl.noaa.gov/psd/enso/data.html [Accessed 31st May 2018].

National Oceanic and Atmospheric Administration National Centers for Environmental Information. (2018) U.S. Climate Divisions. Available at: https://www.ncdc.noaa.gov/monitoring-references/maps/us-climate-divisions.php [Accessed 20th February 2018].

Nickl, E., Willmott, C., Matsuura, K. and Robeson, S. (2010) Changes in annual land-surface precipitation over the twentieth and early twenty-first century. *Annals of the Association of American Geographers*, 100, 729–739. https://doi.org/10.1080/00045608.2010.500241.

Nogueira, R. and Keim, B. (2010) Annual volume and area variations in tropical cyclone rainfall over the eastern United States. *Journal of Climate*, 23, 4363–4374. https://doi.org/10.1175/2010JCLI3443.1.

O'Gorman, P.A. and Schneider, T. (2009) The physical basis for increases in precipitation extremes in simulations of 21st-century climate change. *Proceedings of the National Academy of Sciences of the United States of America*, 106, 14773–14777. https://doi.org/10.1073/pnas.0907610106.

Pan, Z., Liu, X., Kumar, S., Gao, Z. and Kinter, J. (2013) Intermodel variability and mechanism attribution of central and southeastern U.S. anomalous cooling in the twentieth century as simulated by CMIP5 models. *Journal of Climate*, 26, 6215–6237. https://doi.org/10.1175/JCLI-D-12-00559.1.

Pathirana, A., Denekew, H., Veerbeek, W., Zevenbergen, C. and Banda, A. (2014) Impact of urban growth-driven landuse change on microclimate and extreme precipitation—a sensitivity study. *Atmospheric Research*, 138, 59–72. https://doi.org/10.1016/j.atmosres.2013.10.005.

Powell, E. and Keim, B. (2015) Trends in daily temperature and precipitation extremes for the southeastern United States: 1948–2012. *Journal of Climate*, 28, 1592–1612. https://doi.org/10.1175/JCLI-D-14-00410.1.

Prein, A.F., Rasmussen, R.M., Ikeda, K., Liu, C., Clark, M.P. and Holland, G.J. (2016) The future intensification of hourly precipitation extremes. *Nature Climate Change*, 7, 1–6. https://doi.org/10.1038/NCLIMATE3168.

Prein, F.P., Liu, C., Ikeda, K., Trier, S.B., Rasmussen, R.M., Holland, G.J. and Clark, M.P. (2017) Increased rainfall volume from future convective storms in the US. *Nature Climate Change*, 7, 880–884. https://doi.org/10.1038/s41558-017-0007-7.

Rogers, J. (2013) The 20th century cooling trend over the southeastern United States. *Climate Dynamics*, 40, 341–352. https://doi.org/10.1007/s00382-012-1437-6.

Schumacher, R.S. and Johnson, R.H. (2006) Characteristics of US extreme rain events during 1999–2003. *Weather and Forecasting*, 21, 69–85. https://doi.org/10.1175/WAF900.1.

Senkbeil, J. C., Brommer, D. M., & Comstock, I. J. (2011) Hydrometeorological application of an extratropical cyclone classification scheme in the southern United States. *Theoretical and Applied Climatology*, 27-38. https://doi.org/https://doi.org/10.1007/s00704-011-0562-1.

Senkbeil, J.C., Saunders, M.E. and Taylor, B. (2017) Changes in summer weather type frequency in eastern North America. *Annals of the American Association of Geographers*, 107, 1229–1245. https://doi.org/10.1080/24694452.2017.1295839.

Sheridan, S. (2002) The redevelopment of a weather type classification scheme for North America. *International Journal of Climatology*, 22, 51–68. https://doi.org/10.1002/joc.709.

Sugiyama, M., Shiogama, H. and Emori, S. (2010) Precipitation extreme changes exceeding moisture content increases in MIROC and IPCC climate models. *Proceedings of the National Academy of Sciences of the United States of America*, 107, 571–575. https://doi.org/10.1073/pnas.0903186107.

Tootle, G., Piechota, T. and Singh, A. (2005) Coupled oceanic–atmospheric variability and U.S. streamflow. *Water Resources Research*, 41, 1–11. https://doi.org/10.1029/2005WR004381.

Trenberth, K.E., Dai, A., Rasmussen, R. and Parsons, D. (2003) The changing character of precipitation. *Bulletin of the American Meteorological Society*, 84, 1205–1217. https://doi.org/10.1175/BAMS-84-9-1205.

Trepanier, J., Roberts, M. and Keim, B. (2015) Trends and spatial variability in dry spells across the south-central United States. *Journal of Applied Meteorology and Climatology*, 54, 2261–2272. https://doi.org/10.1175/JAMC-D-14-0319.1.

Vecchi, G. A., & Knutson, T. R. (2011) Estimating annual numbers of atlantic hurricanes missing from the HURDAT database (1878-1965) using ship track density. *Journal of Climate*, 1736-1746. https://doi.org/https://doi.org/10.1175/2010JCLI3810.1.

Wright, D., Knutson, T. and Smith, J. (2015) Regional climate model projections of rainfall from US landfalling tropical cyclones. *Climate Dynamics*, 45, 3365–3379. https://doi.org/10.1007/s00382-015-2544-y.

Zhou, Y. and Matyas, C. (2017) Spatial characteristics of storm-total rainfall swaths associated with tropical cyclones over the eastern United States. *International Journal of Climatology*, 37, 557–569. https://doi.org/10.1002/joc.5021.

How to cite this article: Skeeter WJ, Senkbeil JC, Keellings DJ. Spatial and temporal changes in the frequency and magnitude of intense precipitation events in the southeastern United States. *Int J Climatol*. 2018;1–15. https://doi.org/10.1002/joc.5841